Received: 22 March 2019 | Revised: 22 March 2019 | Accepted: 25 July 2019

DOI: 10.1096/fba.2019-00027

RESEARCH ARTICLE

FASEB BioAdvances WILEY

Cyclosporine A inhibits MRTF-SRF signaling through Na^+/K^+ ATPase inhibition and actin remodeling

Bastien Burat[1] | Quentin Faucher[1] | Petra Čechová[2,3] | Hélène Arnion[1] | Florent Di Meo[1] | François-Ludovic Sauvage[1] | Pierre Marquet[1,4] | Marie Essig[1]

[1]Centre for Biology & Health Research, UMR INSERM 1248 IPPRIT (Individual Profiling and Prevention of RIsks in Transplantation), Limoges University, Limoges, France

[2]Department of Biophysics, Centre of the Region Haná for Biotechnological and Agricultural Research, Faculty of Science, Palacký University Olomouc, Olomouc, Czech Republic

[3]Department of Physical Chemistry, Regional Centre of Advanced Technologies and Materials, Faculty of Science, Palacký University Olomouc, Olomouc, Czech Republic

[4]Department of Pharmacology and Toxicology, Limoges University Hospital, Limoges, France

Correspondence
Bastien Burat, Centre for Biology & Health Research, UMR INSERM 1248 IPPRIT (Individual Profiling and Prevention of

Abstract

Calcineurin inhibitors (CNI) are the pillars of immunosuppression in transplantation. However, they display a potent nephrotoxicity whose mechanisms remained widely unsolved. We used an untargeted quantitative proteomic approach (iTRAQ technology) to highlight new targets of CNI in renal proximal tubular cells (RPTCs). CNI-treated RPTCs proteome displayed an over-representation of actin-binding proteins with a CNI-specific expression profile. Cyclosporine A (CsA) induced F-actin remodeling and depolymerization, decreased F-actin-stabilizing, polymerization-promoting cofilin (CFL) oligomers, and inhibited the G-actin-regulated serum response factor (SRF) pathway. Inhibition of CFL canonical phosphorylation pathway reproduced CsA effects; however, S3-R, an analogue of the phosphorylation site of CFL prevented the effects of CsA which suggests that CsA acted independently from the canonical CFL regulation. CFL is known to be regulated by the Na^+/K^+-ATPase. Molecular docking calculations identified two inhibiting sites of CsA on Na^+/K^+-ATPase and a 23% decrease in Na^+/K^+-ATPase activity of RPTCs was observed with CsA. Ouabain, a specific inhibitor of Na^+/K^+-ATPase also reproduced CsA

Abbreviations: 1-way ANOVA, one-way ANalysis Of Variance; α-SMA, α-smooth muscle actin; ABP, actin-binding protein; ACN, acetonitrile; ADP, Adenosine DiPhosphate; BLOTTO, bovine lacto transfer technique optimizer; CAI, cyclophilin A inhibitor; CFL, cofilin; CiR-C, customizable iTRAQ ratio calculator; CNI, calcineurin inhibitors; CsA, cyclosporine A; CypA, cyclophilin A; DAPI, 4′,6-diamidino-2-phenylindole; DMEM-F12, Dulbecco's Modified Eagle's Medium-Ham's F12; DMSO, dimethyl sulfoxide; EDTA, ethylenediaminetetraacetic acid; EGTA, ethylene glycol-bis(β-aminoethyl ether)-N,N,N′,N′-tetraacetic acid; FA, formic acid; FBS, fetal bovine serum; FKBP12, FK506-binding protein 12 kDa; HEPES, 4-(2-hydroxyethyl)-1-piperazineethanesulfonic acid; IDA, information-dependent acquisition; IEF, isoelectric focusing; IPG, immobilized pH gradient; iTRAQ, isobaric tags for relative & absolute quantitation; LIMK, LIM domain kinase; LIMKi3, LIM domain kinase inhibitor 3; LLC PK-1, Lilly Laboratories Cells Porcine Kidney-1; MOPS, 3-(N-morpholino)propanesulfonic acid; MRTF, myocardin-related transcription factor; MS/MS, tandem mass spectrometry; Na+/K+, ATPase sodium/potassium adenosine triphosphatase; nanoHPLC / nanoLC, nano-scale High-Performance Liquid Chromatography; NC, nitrocellulose; NFAT, nuclear factor of activated T-Cells; OUA, Ouabain; PANTHER, Protein ANalysis Through Evolutionary Relationships; PBS, phosphate buffer saline; Pi, inorganic phosphate; PIP2, phosphatidylinositol-4,5-bisphosphate; PLIP, protein-ligand interaction profiler; PPIase, peptidyl-prolyl cis-trans isomerase; PTCs, proximal tubular cells; QqTOF MS, Quadrupole-quadrupole-Time-of-Flight Mass Spectrometry; Rac1, Ras-related C3 botulinum toxin substrate 1; RhoGTPases, Rho Guanidine Triphosphatases; RIPA, buffer radioimmunoprecipitation assay buffer; ROCK, rho-associated, coiled-coil-containing protein kinase; RPTCs, renal proximal tubular cells; S.D., standard deviation; SDS, sodium dodecyl sulfate; SILAC, stable isotope labeling by amino acids in cell culture; SRE, serum response element; SRF, serum response factor; SRF-RE, serum response factor-response element; STRING, Search Tool for the Retrieval of Interacting Genes/Proteins; Tac, tacrolimus; TBS-T, buffer TBS-Tween buffer; TPI, triose phosphate isomerase; TRIS, Tris(hydroxymethyl)aminomethane; TRITC, TetramethylRhodamine IsoThioCyanate.

RIsks in Transplantation), Limoges University, Limoges, France.
Email: bastien.burat@etu.unilim.fr

Funding information
National Program of Sustainability I, MEYS, Grant/Award Number: LO1204

effects on actin organization and SRF activity. Altogether, these results described a new original pathway explaining CsA nephrotoxicity.

KEYWORDS
actin cytoskeleton, cofilin, cyclosporine A, MRTF-SRF, Na^+/K^+-ATPase

1 | INTRODUCTION

The development of immunosuppressive regimens based on the calcineurin inhibitors (CNI), namely cyclosporine A (CsA) and tacrolimus (Tac), has been a breakthrough in the prevention of allograft rejection in solid organ transplantation.[1-3] Although CNI are now widely used in clinical protocols of immunosuppression[4,5] and have significantly improved short-term graft and patient survival, long-term exposure is associated with major limiting deleterious side effects such as nephrotoxicity, leading to end-stage renal disease.[6]

Calcineurin inhibitors nephrotoxicity evolves from acute, reversible vascular, and hemodynamic impairments to chronic irreversible and generalized renal injuries.[7,8] In particular, chronic CNI nephrotoxicity results in interstitial fibrosis and tubular atrophy (IF/TA) of proximal tubules, whose mechanisms remain largely unsolved. Up to now, CNI are known to: disrupt cell cycle and induce cell death[9-14]; induce endoplasmic reticulum stress and unfolded protein response[15-19]; promote oxidative stress[20,21]; impact ion homeostasis[22] or induce epithelial-mesenchymal transition (EMT).[23-25]

These observations resulting from targeted experimental approaches only partially described CNI cell toxicity and do not allow a complete understanding of all the pathophysiological mechanisms at stake. Because the mechanisms of CNI side effects remain widely unsolved by targeted strategies, the design of untargeted experiments is of utmost importance to gain new insights and improve knowledge about the pathophysiology of CNI proximal tubule cell (PTCs) toxicity.

Omics based on the high-throughput analysis of biological systems such as Shotgun proteomics seem particularly well suited to this purpose. In this study, we performed the quantitative proteomic analysis and dynamic mapping of CNI-exposed PTC proteome to elucidate new intracellular pathways specifically modified under CNI exposure.

Upon the significant over-representation and differential expression of actin family cytoskeletal proteins, we focused on the deciphering of the intracellular mechanisms of CsA-induced reorganization of the actin cytoskeleton of PTC and its downstream consequences. We showed that CsA induced an inhibition of the actin-dependent myocardin-related transcription factors-serum response factor (MRTF-SRF) transcription activity through an original regulation of cofilin (CFL) by the Na^+/K^+-ATPase.

2 | MATERIALS AND METHODS

2.1 | Chemicals

Dulbecco's Modified Eagle's Medium-Ham's F12 (DMEM-F12 1:1, #31331, Gibco), fetal bovine serum (FBS, #10500), 1 mol/L HEPES (#15630), 7.5% Sodium bicarbonate (#25080), 10 000 UI/mL Penicillin/Streptomycin (#15140), 0.05% Trypsin-EDTA (#25300-054) Dulbecco's phosphate-buffered saline (PBS, #14190) were purchased from Gibco. Sodium selenite (#S5261), CsA (#30024), Tac (#F4679), Jasplakinolide (#J4580), Latrunculin A (#L5163), ROCK inhibitor Y27632 (#Y0503), Rac1 inhibitor EHT 1864 (#E1657), Alamethicin (#A4665), Digitonin (#D141), ATP (#A1852) Na^+/K^+-ATPase inhibitor Ouabain (#O3125), insulin (#I4011), triiodothyronine (#T6397), dexamethasone (#D4902), Protease Inhibitor Cocktail (#P8340), and Phosphatase Inhibitor Cocktail 2 (#P5726) were purchased from Sigma-Aldrich. Cyclophilin A inhibitor (#239836, Calbiochem) was purchased from Millipore. LIMK1/2 inhibitor LIMKi3 (#4745) was provided by Tocris.

S3-R peptide (MASGVMVSDDVVKVFNRRRRRRRRR), an analogue of the Cofilin phosphorylation site, was synthetized by ProteoGenix.

2.2 | Cell culture conditions

Lilly Laboratories Cells Porcine Kidney-1 (LLC PK-1) porcine PTCs (ATCC-CL-101, ATCC) were expanded in 75 cm^2 flasks at 37°C with 5% CO_2 and passed once confluence was reached. Culture medium consisted in a 1:1 DMEM-F12 mix supplemented with 5% FBS, 15 mmol/L HEPES, 0.1% Sodium bicarbonate, 100 UI/mL Penicillin/Streptomycin and 50 nmol/L Sodium selenite. Passages were performed with 0.05% Trypsin-EDTA. LLC PK-1 cells were cultured between passage 7 and passage 30.

Seeded LLC PK-1 sustained serum starvation and were fed with hormonally-defined (25 µg/mL insulin, 11 µg/mL transferrin, 50 nmol/L triiodothyronine, 0.1 µmol/L dexamethasone, 0.1 µg/mL desmopressin) fresh medium to engage epithelial differentiation, for 24 hours.

Hormonally-defined LLC PK-1 cells sustained cell transfection or were exposed for 24 hours to: vehicle mix (Ethanol, DMSO), 5 µmol/L CsA, 0.05 µmol/L Tac, 1 µmol/L VIVIT (a specific NFAT inhibitor), 0.5 µmol/L cyclophilin A

inhibitor, 200 nmol/L Jasplakinolide, 100 nmol/L Latrunculin A,10 μmol/L ROCK inhibitor Y27632, Rac1 inhibitor EHT 1864, and LIMK inhibitor LIMKi3, 100 nmol/L Na^+/K^+-ATPase inhibitor Ouabain or 100 μg/L S3-R.

2.3 | Actin cytoskeleton characterization

2.3.1 | Immunocytochemistry

Serum-starved, hormonally defined, treated LLC PK-1 cells seeded on glass cover slips in six-well plates were washed twice for 3 minutes in PBS. Then, cells were fixed in 4% paraformaldehyde-PBS for 10 minutes, at room temperature. Cells were washed once again in PBS for 3 minutes then permeabilized with 0.1% Triton/X-100-PBS for 5 minutes, at room temperature. Permeabilized cells were washed three times for 3 minutes in PBS before incubation in Phalloidin-TRITC-PBS for 30 minutes, at 37°C, in the dark. Eventually, cover slips were washed three times for 3 minutes in PBS then mounted on glass microscope slides using ProLong® Gold Antifade Reagent as a mounting medium and a DAPI nuclei staining. Florescence labeling was visualized using a Leica DM-RX microscope (16 × 40).

2.3.2 | Image analysis

For each exposure condition, 10 photographs (*.tiff) were randomly taken to report from an independent experiment. Image analysis was conducted using the ImageJ software (v.1.48). Early image processing consisted in a restriction to the green channel of the RGB picture. The implemented Auto Local Threshold tool further selected the fluorescence-positive pixels (Niblack thresholding method, radius = 15). Thus, for each photograph, a semi-quantitative ratio was calculated as a percentage of the total image area.

All steps mentioned above were automatized thanks to the macro editing tool of the ImageJ software.

2.4 | Luciferase gene reporter assay for SRF/SRE activity

2.4.1 | Stable cell transfection and clone selection

Volumes equivalent to 0, 2, or 4 μg of plasmid DNA (pGL4.34[luc2P/SRF-RE/Hygro] Vector, Promega) and transfection reagent lipofectamine (1:25, Lipofectamine™ 2000 Transfection Reagent, Invitrogen) were separately diluted in FBS-free, antibiotic-free routine medium. Then, DNA and lipofectamine preparations were blended and put at rest for 15 minutes, at room temperature. Serum-starved, hormonally defined LLC PK-1 cells in six-well plates were incubated with DNA-lipofectamine mixtures for 24 hours, at 37°C.

Transfected LLC PK-1 cells (LLC PK-1 SRE) were incubated in routine medium for 72 hours before antibiotic selection to allow proper plasmid integration. Then, cells were re-suspended in 0.05% Trypsin-EDTA, 10 minutes at 37°C. Cell suspensions were diluted 10 times and re-seeded in routine medium completed with 1% Hygromycin B (50 mg/mL) refreshed every 48 hours until colonies appear. Colonies were harvested thanks to trypsin-soaked paper disks (#Z374431, Sigma-Aldrich) and re-seeded to start routine culture in antibiotic-supplemented growth medium.

2.4.2 | Luciferase gene reporter assay/ Bioluminescence assay

Serum-starved, hormonally defined, treated LLC PK-1 SRE were re-suspended mechanically in 1× lysis buffer (Cell Culture Lysis 5X Reagent, #E153A, Promega). Cell lysates were distributed in technical duplicates in a white 96-well plate (#3912, Costar). Bioluminescence signals were detected by the Enspire Multimode Reader (Perkin-Elmer). Bioluminescence values were normalized as percentages of the mean bioluminescence value of the control technical duplicates of biological triplicates. Condition-specific transcription activities were calculated as means of normalized values obtained from condition-related technical duplicates of biological triplicates.

2.5 | Oligomer cross-linking and Western blot

Serum-starved, hormonally-defined, treated LLC PK-1 cells in 60 mm Petri dishes were incubated in hormonally defined medium—1% formaldehyde (cross-linking range 2.9 Å) for 15 minutes under agitation. Formaldehyde cross-linking was quenched by the addition of 1 mol/L glycine (final concentration 125 mmol/L). LLC PK-1 were washed twice with PBS and lysed by scrapping in a custom RIPA lysis buffer (150 mmol/L NaCl, 50 mmol/L TRIS-HCl, 0.1% NP-40, 0.1% SDS, 1 mmol/L EDTA in ultrapure H_2O, supplemented with a 1:100 antiprotease/antiphosphatase mix). Cell lysates were incubated on ice for 30 minutes and centrifuged for 15 minutes at 21 000 g. Supernatants were stored until protein concentration was measured using the Bradford colorimetric method. Forty micrograms of proteins per exposure condition was separated by electrophoresis under reducing and denaturing conditions on a NuPAGE® 12% Bis-Tris pre-cast gel (#NP0341; ThermoFisher) in 1× NuPAGE™ MOPS SDS running buffer (#NP0001; ThermoFisher) and transferred to a nitrocellulose (NC) membrane (NP23001; ThermoFisher) using the iBLOT 2 Dry Blotting system (#IB21001; ThermoFisher). Membranes were stained with 0.1% Ponceau S, 5% acetic acid solution for total protein visualization. Membranes were blocked for 1 hour at room

temperature under agitation with TBS-Tween (TBS-T) buffer (10 mmol/L Tris 7.6, 150 mmol/L NaCl, 0.1% Tween-20) complemented with 5% (W/V) non-fat milk powder to obtain BLOTTO buffer. Primary antibody incubation (anti-CFL, 1:10 000, #PA1-24931, ThermoFisher) was done in BLOTTO for 1 hour at room temperature. After three 5-minute washes in TBS-T, secondary antibody incubation (F(ab')2-Goat anti-Rabbit IgG (H + L) Secondary Antibody, HRP, 1:10 000, #A24531, ThermoFisher) was performed in BLOTTO for 1 hour at room temperature then washed again. Membranes were incubated in a 1:1 mix of SuperSignal™ West Pico PLUS Chemiluminescent Substrate kit (#34577, ThermoFisher) and analyzed by the ChemiDoc Imaging system (Bio-Rad) for chemiluminescent signal detection and acquisition. Quantitation was computed via the ImageLab software (Bio-Rad) after total protein normalization.

2.6 | Na^+/K^+-ATPase activity/phosphate release assay

Serum-starved, hormonally defined, treated LLC PK-1 cells in 24-well plates were permeabilized by osmotic shock in ultrapure water (150 µL) and fast freeze in liquid nitrogen (10 seconds). Cells were thawed (200 µL) in a buffer with a composition of 200 mmol/L sodium chloride, 80 mmol/L histidine, 20 mmol/L potassium chloride, 6 mmol/L magnesium chloride, 2 mm EGTA, 2 µg/mL Alamethicin, 30 µmol/L Digitonin. For each drug exposure condition, a volume of 30 mmol/L Ouabain (final concentration 1 mmol/L) or ultrapure water was added to every other well. Cells were either incubated 30 minutes at 37°C. A volume of 30 mmol/L ATP (final concentration 1 mmol/L) was added to each well. Cells were incubated 30 minutes more at 37°C. On ice, trichloroacetic acid: water (1:1) terminated ATP hydrolysis reactions. Plates were centrifuged at 1200 *g* for 10 minutes at room temperature. Supernatants were diluted 50 times and distributed (50 µL) in technical triplicates to a 96-well plate.

Concentration of free phosphate released from ATP hydrolysis was measured using the BIOMOL® Green kit (BML-AK-111-0250, Enzo). Na^+/K^+-ATPase activity (expressed in nmol of released phosphate/30min/105 cells) was calculated as the difference in free phosphate concentration in the presence and absence of Ouabain.

2.7 | iTRAQ shotgun proteomics

2.7.1 | Protein extraction, sample preparation, iTRAQ labeling, and isoelectric focusing

After 24 hours drug exposure, LLC PK-1 cells were washed twice with PBS and lysed by scrapping in a custom RIPA lysis buffer (150 mmol/L NaCl, 50 mmol/L TRIS-HCl, 0.1% NP-40, 0.1% SDS, 1 mmol/L EDTA in ultrapure H_2O, supplemented with an antiprotease/ antiphosphatase mix). Cell lysates were incubated on ice for 30 minutes and centrifuged for 15 minutes at 21 000 *g*. Supernatants were stored until protein concentration was measured using the Bradford colorimetric method and iTRAQ labeling. Twenty-five micrograms of proteins was precipitated by −20°C cold acetone. After acetone evaporation, the precipitates were solubilized in 25 mmol/L ammonium bicarbonate then were incubated with 50 mmol/L dithiothreitol for 40 minutes at 60°C, to reduce disulfide bonds, 100 mmol/L iodoacetamide in the dark for 40 minutes at room temperature, to alkylate/block cysteine residues and eventually were digested for 24 hours at 37°C with mass-spectrometry grade trypsin (#V5280; Promega) at a 1:50 enzyme: substrate ratio.

After digestion, samples were incubated with iTRAQ tags (iTRAQ Reagents Multi-plex kits, 4-plex, #4352135; Sigma-Aldrich)—one tag per drug exposure condition and five different tag/condition associations over five experiments—for 1 hour at room temperature. Labeled samples were mixed and separated into 12 fractions by isoelectric focusing (OFFGEL 3100 Fractionator; Agilent Technologies) for 24 hours at increasing voltage and steady intensity of 50 µA in a 3-10 pH IPG strip. Fractions were retrieved for further MS analysis after the IPG strip was incubated in a 1:1 acetonitrile (ACN): water, 0.1% formic acid (FA) wash solution for 15 minutes at room temperature.

2.7.2 | Nano-LC peptide separation and Q-Q-TOF mass spectrometry

IEF fractions were analyzed by nano-LC MS/MS using a nano-chromatography liquid Ultimate 3000 system (LC Packings DIONEX) coupled to a Triple TOF 5600+ mass spectrometer (ABSciex). For each sample, 5 µL was injected into a pre-column (C18 Pepmap™ 300 µm ID × 5 mm, LC Packings DIONEX) using the loading unit. After desalting for 3 minutes with loading solvent (2% ACN, 0.05% trifluoroacetic acid [TFA]), the pre-column was switched online with the analytical column (C18 Pepmap™ 75 µm ID × 150 mm, LC Packings DIONEX) pre-equilibrated with 95% solvent A (ACN 5%—FA 0.1%). Peptides were eluted from the pre-column into the analytical column and then into the mass spectrometer by a linear gradient from 5% to 25% in 70 minutes, then to 95% of solvent B (98% ACN, 0.1% FA) over 120 minutes at a flow rate of 200 nL/min.

Data acquisition was carried out by IDA (Information-Dependent Acquisition) mode of Analyst 1.7 TF software (ABSciex). The data from MS and MS/MS were continuously recorded with a cyclic duration of 3 seconds. For each MS scan, up to 50 precursors were selected for fragmentation based on their intensity (greater than 20 000 cps), their charge state (2+, 3+) and if the precursor had already been selected

for fragmentation (dynamic exclusion). The collision energies were automatically adjusted according to charge state, ionic mass of selected precursors, and iTRAQ labeling.

2.7.3 | Mass spectrometry data processing and relative protein identification/quantification

MS and MS/MS data for five independent experiments (biological replicates) (*.wiff, one per fraction, 12 files per experiment) were submitted to Mascot Server 2.2.03 via ProteinPilot (version 5.0, ABSciex) for protein identification, and searched against two complementary *Sus scrofa* databases: a Swiss-Prot database (2015_10 release) and a TrEMBL database (2015_10 release). Carbamidomethyl (C) was defined as a fixed modification. Oxidation (O), iTRAQ4plex (K), iTRAQ4plex (Y), and iTRAQ4plex (N-term) were defined as variable modifications. MS/MS fragment mass tolerance was set at 0.3 Da. Precursor mass tolerance was set at 0.2 Da.

Mascot raw data files (*.dat, one per experiment) were saved for further isobaric tags-based peptide and protein quantitation with the Java implementation of the Quant algorithm, jTRAQx (version 1.13[26]). Reporter mass tolerance was set at 0.05 Da, whereas iTRAQ correction factors were implemented as provided by ABSciex. This tool generated one *.jpf file (tab-delimited text file) for each series.

*.jpf were submitted to the CiR-C (Customizable iTRAQ Ratio Calculator) algorithm which excluded irrelevant data according to: (a) identification confidence: peptides are retained if the probability that the observed positive match is a random match is below 5% ($P < .05$, Mascot score > 30); (b) quantification confidence: peptides are retained if all iTRAQ ratios have been successfully calculated ie, peptides with 0.0 ratios or uncalculated ratios (null ratios) are discarded; (c) peptides related to "Fragment"- and "REVERSED"-annotated proteins are discarded. After irrelevant data removal, CiR-C drew up an exhaustive catalogue of identified peptide sequences with their associated Swiss-Prot or TrEMBL accession IDs. Peptides were assigned to a frequency index of positive matches (identification in {1;2;3;4;5} of five independent experiments) and CiR-C drew a second catalogue of peptides with the highest frequency index (n = 5). Protein ratios were calculated as both overall and series-specific median values of peptide ratios associated with a given accession ID and frequency index.

2.7.4 | PANTHER overrepresentation test

The protein list analysis was performed by submitting Swiss-Prot accession IDs to the online tool powered by the PANTHER Classification system. The PANTHER Overrepresentation test (release date 13/04/2017) parsed the PANTHER database (version 12.0, released on 10/07/2017) using the *Sus scrofa* reference list and the PANTHER Protein Class annotation dataset. Only $P < .05$ items were retained and considered significantly over-represented.

2.7.5 | Visualization of protein networks

The visualization of protein networks was performed by submitting Swiss-Prot accession IDs to the online tool STRING.

2.7.6 | Biological significance criteria

Frequency distribution of the iTRAQ peak intensities ratios could be approximated as a Gaussian distribution: iTRAQ peak intensities ratios frequency distribution significantly fitted implemented Gaussian nonlinear regression (n = 370, $R^2 = 0.9946$, mean = 1.02 ± 0.10). One of the Gaussian distribution properties is: (a) 66% of the values lie in a 1 SD range around the mean; (b) 95% of the values lie in a 2 SD range around the mean; (c) 99% of the values lie in a 3 SD range around the mean. Applying the "mean ± n SD" property to the set of iTRAQ peak intensity ratios, the upper thresholds for significant upregulations upon drug exposure would be "$1.02 - 0.10 = 0.92$," "$1.02 - 2 \times 0.10 = 0.82$," and "$1.02 - 3 \times 0.10 = 0.72$," whereas the lower thresholds for significant downregulations upon drug exposure would be "$1.02 + 0.10 = 1.12$," "$1.02 + 2 \times 0.10 = 1.22$," and "$1.02 + 3 \times 0.10 = 1.32$". Thus, proteins were classified thanks to their distance from the unity: proteins with median ratios between 0.92 and 1.12 were annotated as non-impacted proteins; upregulated proteins with quantitative ratios beyond 1.12 were ranked according to three tiers of significant fold increase: $+\sigma$ ($1.12 \leq r < 1.22$), $+2\sigma$ ($1.22 \leq r < 1.32$), or $+ 3\sigma$ ($1.32 \leq r$). The same way downregulated proteins with quantitative ratios below 0.82 were ranked according to three tiers of significant fold decrease: $-\sigma$ ($0.92 \geq r > 0.82$), -2σ ($0.82 \geq r > 0.72$), or -3σ ($0.72 \geq r$).

2.7.7 | Hierarchical clustering & heat-map representation

Heat map representation and hierarchical clustering were generated using the Euclidian distance calculation as provided by the GENE-E software (version 3.0.204).

2.8 | Data availability

The MS proteomics data have been deposited to the ProteomeXchange Consortium (http://proteomecentral.proteomexchange.org)[27] via the PRIDE partner repository[28] with the dataset identifier PXD007891 (username: reviewer72095@ebi.ac.uk, password: TPSGICw9).

2.9 | Setup of cyclosporine docking into Na^+/K^+-ATPase

A cyclosporine structure was docked into a human-sequence homology model of Na^+/K^+-ATPase based on crystal structures (PDB IDs: 2ZXE and 4HQJ respectively for the open conformation E2 state ([29] and the closed conformation E1 state[30]).

The molecules were prepared for docking in Autodock Tools[31] and the docking was performed in Autodock Vina[32] with grid covering the whole protein and exhaustiveness set to 400. A second docking was performed into the lipid-binding site C to better evaluate the cyclosporine binding in this position.

The docking was performed in three variations, with 20 binding poses generated for each case: (a) the closed structure E1 with a bound ATP molecule; (b) the closed structure E1 without ATP; (c) the open structure E2 without phosphate.

Given the similarity of the docking results between the closed conformation with and without ATP, and the experimental conditions, only the results of the docking with ATP are presented. The residues taking part in ligand binding were evaluated using PLIP.[33] Figures were made using PyMOL (The PyMOL Molecular Graphics System, Version 1.6, Schrödinger, LLC).

2.10 | Statistics

Statistical analysis and comparison of positive fluorescence area, SRF-MRTF transcription activity, relative CFL abundance and Na^+/K^+-ATPase activity data were performed using the one-sample *t* test for versus control comparison and the one-way ANOVA test followed by the adequate multiple comparison post-test with a significance threshold at $P < .05$, as implemented in GraphPad Prism (v. 5.04).

3 | RESULTS

3.1 | Quantitative proteomic analysis of PTC proteome & mapping of CNI-induced perturbations highlight the over-representation and differential expression of actin family cytoskeletal proteins

To monitor the dynamic profile of CNI-exposed PTC proteome, proteins extracted from LLC PK-1 cell lysates, after 24-hour exposure to CNI, were prepared for shotgun proteomics combining iTRAQ labeling of tryptic peptides to nanoHPLC-QqTOF MS analysis.

TABLE 1 Cytoskeletal proteins are significantly overrepresented in the proteome of calcineurin inhibitors-exposed Lilly Laboratories Porcine Kidney-1 monitored by iTRAQ shotgun proteomics. Swiss-Prot IDs from 128 identified proteins were submitted to the PANTHER Overrepresentation test (release date 13/04/2017) parsing the PANTHER database (version 12.0, released on 10/07/2017) using the *Sus scrofa* reference list and the PANTHER Protein Class annotation dataset. Bonferroni correction was applied

PANTHER protein class	Reference proteins per class (/21324)	Input proteins per class (/128)	Expected proteins per class	Over(+)/ under(−)-representation	Fold enrichment	*P*-value
Tubulin (PC00228)	20	4	0.12	+	33.32	1.51×10^{-3}
Hydratase (PC00120)	16	3	0.10	+	31.24	2.70×10^{-2}
Ribosomal protein (PC00202)	241	23	1.45	+	15.90	1.48×10^{-18}
Dehydrogenase (PC00092)	234	11	1.40	+	7.83	4.19×10^{-5}
Isomerase (PC00135)	131	6	0.79	+	7.63	3.09×10^{-2}
RNA binding protein (PC00031)	681	24	4.09	+	5.87	6.08×10^{-10}
Oxidoreductase (PC00176)	540	19	3.24	+	5.86	1.46×10^{-7}
Actin family cytoskeletal protein (PC00041)	313	10	1.88	+	5.32	4.39×10^{-3}
Cytoskeletal protein (PC00085)	660	15	3.96	+	3.79	2.24×10^{-3}
Nucleic acid binding (PC00171)	2031	28	12.19	+	2.30	4.86×10^{-3}
Unclassified	11 800	31	70.83	−	0.44	0

Analysis type	PANTHER Overrepresentation test (release 13/04/2017)
Annotation version—release date	PANTHER version 12.0 - 2017-07-10
Analyzed list	*Sus scrofa* (128 input proteins)
Reference list	*Sus scrofa* (21 324 reference proteins)
Bonferroni correction	True
Bonferroni count	201

iTRAQ technology allowed the identification of 130 proteins in PTC lysate. The PANTHER over-representation test (Table 1) classified 128 *Sus scrofa* proteins, related to ribosome structure (PC00202, fold enrichment = 15.90, ***P-value = 1.48×10^{-18}), nucleic acid binding (PC00031, fold enrichment = 5.87, ***P-value = 6.08×10^{-10}; PC00171, fold enrichment = 2.30, **P-value = 4.86×10^{-3}), metabolism processes (PC00120, fold enrichment = 31.24, *P-value = 2.70×10^{-2}; PC00092, fold enrichment = 7.83, ***P-value = 4.19×10^{-5}; PC00135, fold enrichment = 7.63, *P-value = 3.09×10^{-2}; PC00176, fold enrichment = 5.86, ***P-value = 1.46×10^{-7}) and cytoskeleton dynamics (PC00228, fold enrichment = 33.32, **P-value = 1.51×10^{-3}; PC00041, fold enrichment = 5.32, **P-value = 4.39×10^{-3}; PC00085, fold enrichment = 3.79, **P-value = 2.24×10^{-3}).

Among the 15 proteins related to cytoskeleton structure and dynamics, actin family cytoskeletal proteins (PANTHER Protein Class PC00041, fold enrichment = 5.32, **P-value = 4.39×10^{-3}) formed a node of 10 interconnected proteins in the visualization of functional protein networks (Figure S1A).

Among the 70 proteins with significant variations of abundance, actin family cytoskeletal proteins like moesin, radixin, myosin VI, α-SMA, troponin-C, F-actin capping protein subunits α2 and β, and cofilin-1 showed a CNI-specific expression profile (Figure S1B).

3.2 | CsA, but not Tac, elicited a strong reorganization of actin cytoskeleton of PTCs

To determine whether CNI-specific variations in the protein abundance of actin family cytoskeletal proteins were related to phenotypic modifications of the actin cytoskeleton, the characterization of LLC PK-1 F-actin microfilaments was performed by Phalloidin-TRITC labeling and fluorescence microscopy, after 24-hour exposure to CNI.

In fluorescence microscopy, cell monolayers of proximal tubular LLC PK-1 showcased a puzzled pattern as phalloidin-labeled F-actin cytoskeleton organized cell membranes into intercellular convolutions (Figure 1A, panel a). These peculiar structuring of plasma membranes were reminiscent of the way basolateral membranes connect inside proximal tubular epithelia, in vivo.

Upon 24-hour CsA exposure, LLC PK-1 sustained a significant reorganization of cortical actin cytoskeleton (Figure 1A, panel b) related to a significant loss of F-actin-based structures (Figure 1B, −0.46%, **$P < .01$). CsA effects seemed to be related to the inhibition of the peptidylprolyl cis-trans isomerase activity of its target immunophilin cyclophilin A (CypA) since a specific pharmacological inhibitor of CypA (CAI), without any immunological effect, elicited similar actin modifications (Figure 1A panel e, Figure 1B, −0.51%, **$P < .01$). On the contrary, CsA effects seemed independent of calcineurin inhibition since neither Tac, VIVIT (a specific inhibitor of NFAT dephosphorylation by calcineurin) nor GPI 1046 (a pharmacological inhibitor of FKBP12) exhibited modifications of the actin organization (Figure 1A panels c, d, and f, Figure 1B).

In conclusion, these observations suggested that CsA triggered the deep remodeling of proximal tubular actin cytoskeleton and the depolymerization of F-actin, in a cyclophilin-dependent way, independently of calcineurin inhibition.

3.3 | Actin depolymerization led to a decrease in MRTF-SRF transcription activity in LLC PK-1 upon CsA exposure

The accumulation of cytoplasmic G-actin is known to prevent MRTF nuclear import and inhibit the transcription activity of the MRTF-SRF complex. To determine CNI effects on MRTF-SRF activity, LLC PK-1 cells were transfected by a vector consisting of the luciferase gene under the control of a MRTF-SRF-activated CArG box-containing promoter for gene reporting of MRTF-SRF transcription activity, after 24-hour exposure to CNI.

Upon 24-hour CsA exposure, SRF transcription activity was significantly reduced (Figure 2 A, −48.5% of control activity, ***$P < .001$). Likewise, CAI elicited a concentration-dependent negative regulation of SRF (Figure 2C). On the contrary, neither Tac, VIVIT (Figure 2B) nor GPI 1046 (Figure 2D) reduced SRF transcription activity which was slightly increased upon Tac and VIVIT exposure. Profiles of drug-related actin dynamics strictly superimposed to profiles of drug-related SRF transcription activity.

In conclusion, CsA downregulated the transcription of MRTF-SRF target genes, in a cyclophilin-dependent way, independently of calcineurin inhibition.

3.4 | CsA regulates actin-binding protein cofilin through changes in cofilin-actin ratio and oligomerization state

The depolymerization of F-actin into G-actin can be catalyzed by actin-depolymerizing factors such as CFL. CFL activity is regulated by its ratio to F-actin and its oligomerization state.

Differential quantitative proteomic analysis of identified actin family cytoskeletal proteins (PANTHER Protein Class PC00041) showed that CsA decreased the CFL: actin ratio since actin was overexpressed, whereas CFL levels remained steady. On the contrary, Tac induced equivalent overexpression for both actin and CFL (Figure S1).

To determine whether CsA exposure induced changes in CFL oligomerization, the Western blot analysis of CFL oligomers from CsA-treated LLC PK-1 cell lysates was performed.

Western blot analysis of cross-linked CFL oligomers (Figure 3A) indicated that CsA induced

a significant decrease in dimers and tetramers ($R_{diCFL} = 0.40 \pm 0.09$; $R_{tetraCFL} = 0.38 \pm 0.16$), whereas monomers remain steady ($R_{monoCFL} = 0.90 \pm 0.06$) (Figure 3B).

In conclusion, CsA elicited a shift in the balance between oligomeric forms of CFL, decreasing the protein abundance of CFL dimers and tetramers.

3.5 | CsA effects seemed partly independent of CFL phosphorylation/dephosphorylation

Another level of CFL regulation is its phosphorylation state. To determine whether CsA effects were related to CFL phosphorylation state, the characterization of LLC PK-1 actin

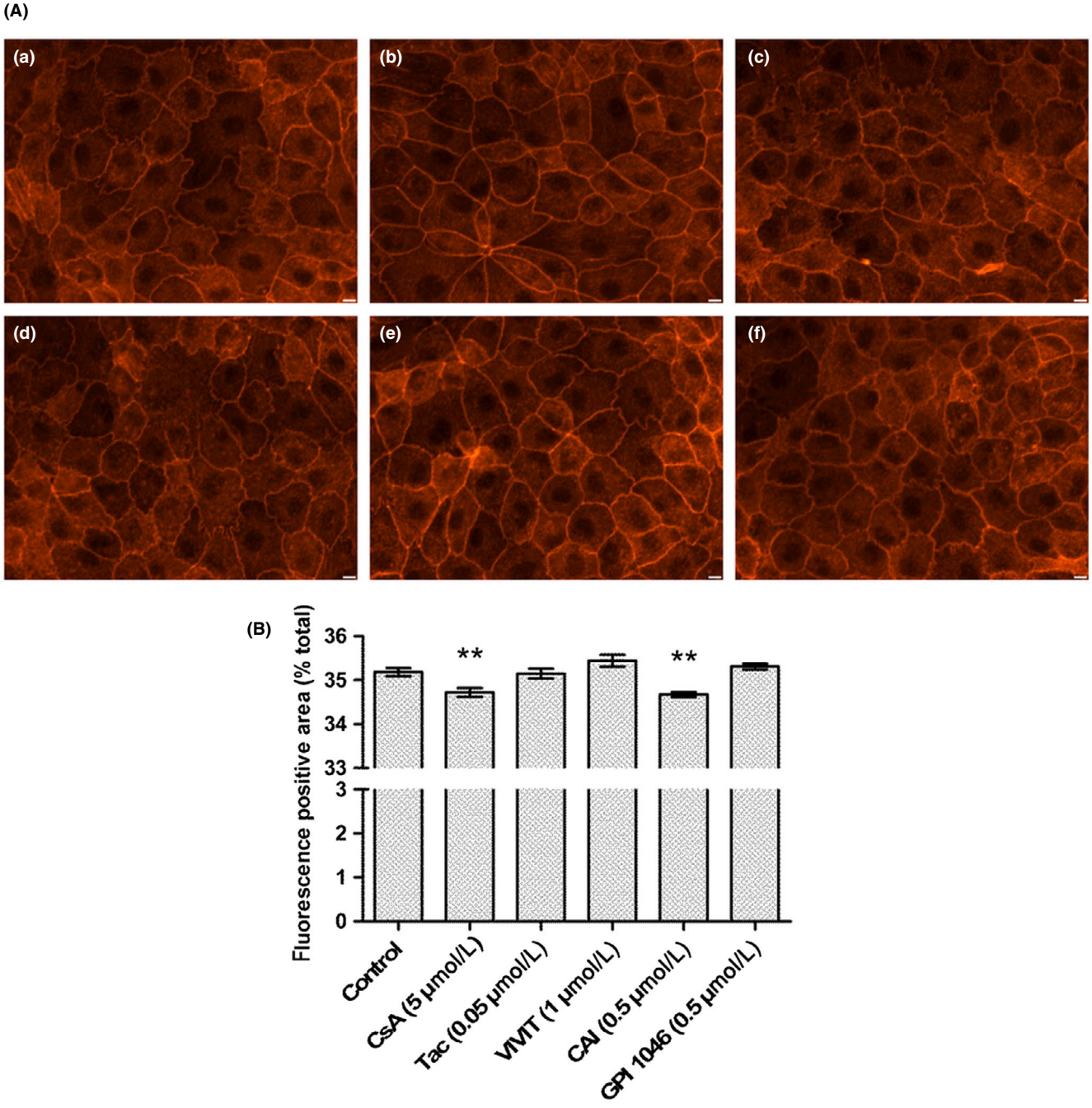

FIGURE 1 Cyclosporine A (CsA), but not tacrolimus (Tac), triggers F-actin depolymerization in a NFAT-independent, immunophilin inhibition-related way. A, Fluorescence images of Lilly Laboratories Porcine Kidney-1 actin cytoskeleton labeled with TRITC-Phalloidin. Scale bar 10 µm. B, Quantification of red fluorescence-positive area. Mean ± SEM. One-way ANOVA plus Dunnett's post-test (**$P < .01$). Drug condition: (a) vehicle (0.5% ethanol) (b) 5 µmol/L CsA (c) 0.05 µmol/L Tac (d) 1 µmol/L VIVIT (e) 0.5 µmol/L CAI (f) 0.5 µmol/L GPI 1046. Exposure time: 24 h (n = 3)

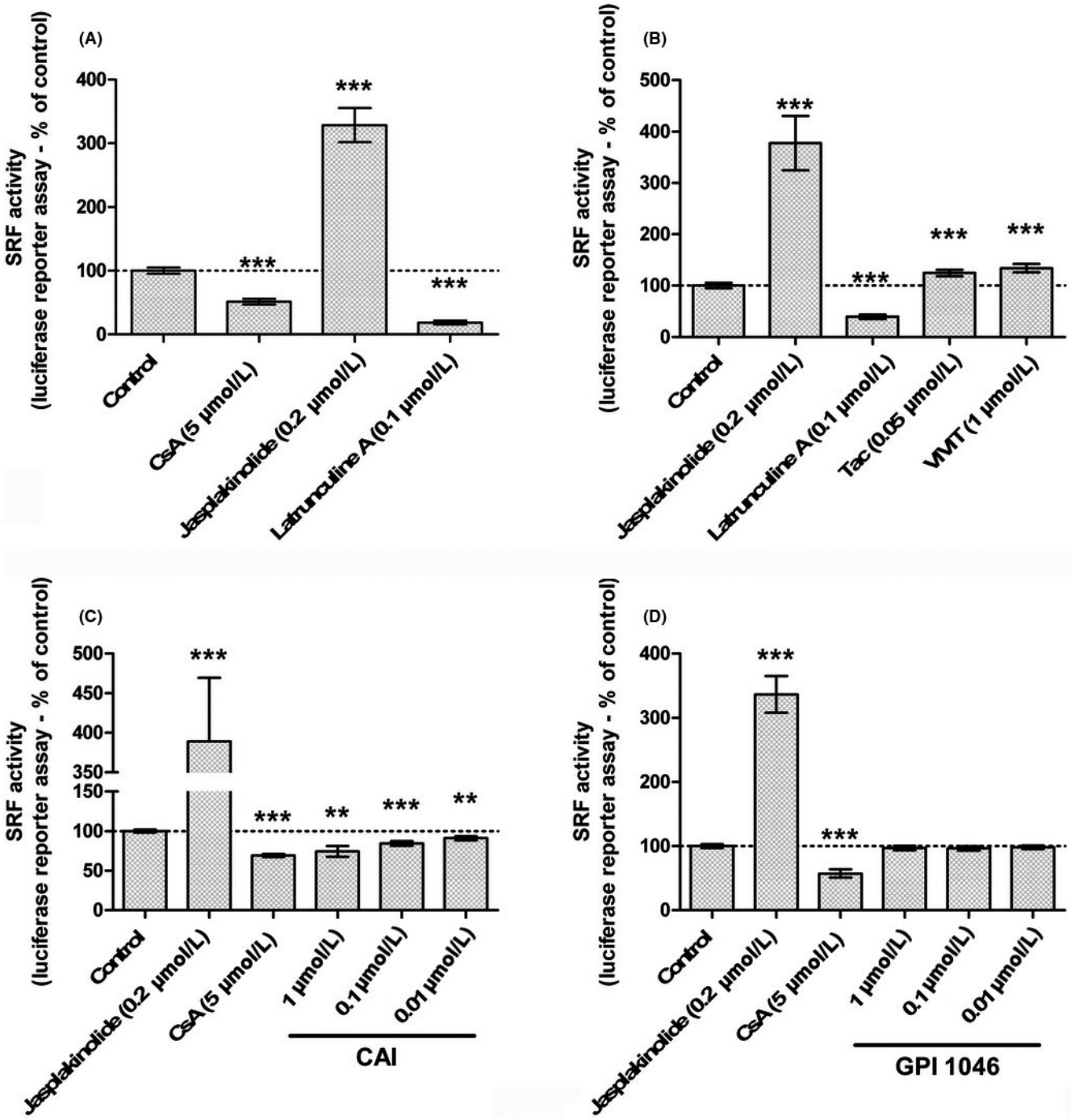

FIGURE 2 Cyclosporine A (CsA)-induced accumulation of G-actin leads to inhibition of serum response factor (SRF)-myocardin-related transcription factor transcription activity in a NFAT-independent, immunophilin inhibition-related way. SRF transcription activity was measured by luciferase gene reporter assay in Lilly Laboratories Porcine Kidney-1 SRE exposed for 24 h to: Drug condition: (A-D). Vehicle (0.5% ethanol-0.2% DMSO), 5 µmol/L CsA, 0.2 µmol/L Jasplakinolide; (A, B) 0.1 µmol/L Latrunculin A; (B) 0.05 µmol/L tacrolimus (Tac), 1 µmol/L VIVIT; (C) 0.01-1 µmol/L CAI, (D) 0.01-1 µmol/L GPI 1046. Mean ± SEM. One-sample *t* test (***P* < .01, ****P* < .001). (A-C, D) (n = 3). (B) (n = 5)

cytoskeleton and MRTF-SRF transcription activity was done after 24 hours exposure to S3-R, a peptide analogue of CFL phosphorylation site, and pharmacological inhibitors of the RhoGTPases pathway, responsible for CFL phosphorylation.

The S3-R peptide, an analogue of the CFL phosphorylation site and a non-specific inhibitor of Ser3-targeting proteins, did not affect the organization of the actin cytoskeleton (Figure 4 A, panel b) but was linked to a slight yet significant increase in F-actin levels (Figure 4B, +0.36%, **P* < .05). In association with CsA, S3-R nullified the CsA-induced actin remodeling (Figure 4A, panel e, Figure 4B). Conversely, the addition of a specific pharmacological inhibitor of LIMK, LIMKi3, alone or associated with CsA triggered CsA-like phenotype of actin dynamics (Figure 4A, panel c and f) and significantly

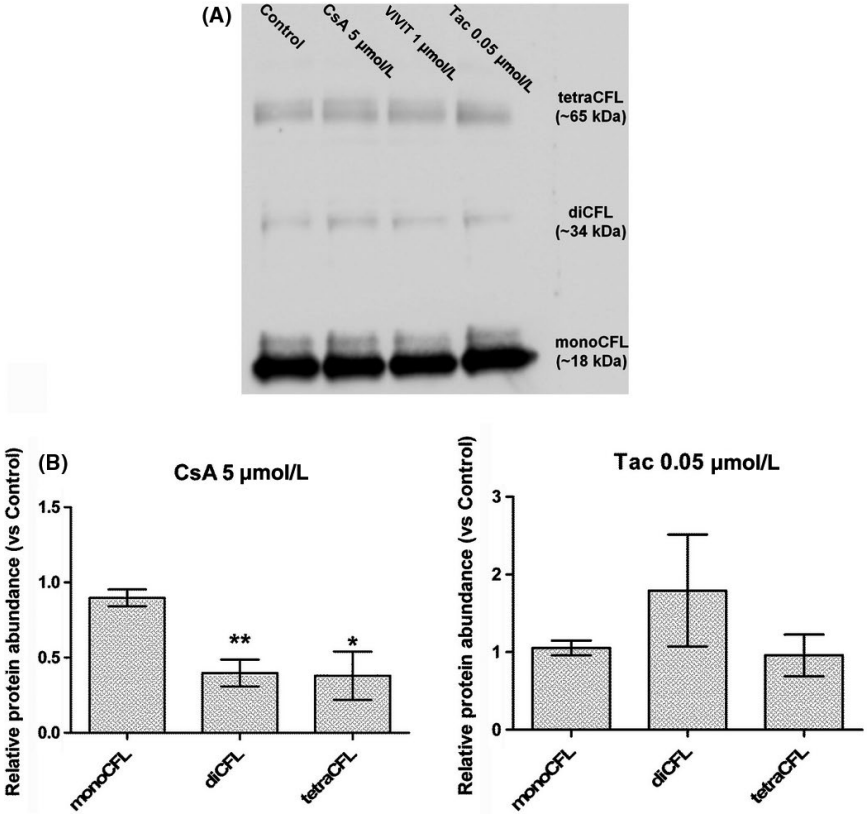

FIGURE 3 Cyclosporine A (CsA), but not tacrolimus (Tac), induced changes in cofilin (CFL) concentration-to-actin. A, Western blot detection of formaldehyde-cross-linked CFL oligomers in Lilly Laboratories Porcine Kidney-1 lysates. B, Quantification of relative protein abundance of CFL oligomeric forms. Mean ± SEM. One-way ANOVA plus Dunnett's post-test (*$P < .05$, **$P < .01$). Drug condition: 5 µmol/L CsA, 0.05 µmol/L Tac. Exposure time: 24 h (n = 5)

decreased F-actin levels (Figure 4B, LIMKi3 alone: −1.62%, ***$P < .001$; LIMKi3 + CsA: −1.22%, ***$P < .001$).

S3-R alone did not impact the MRTF-SRF transcription activity (Figure 5A). In association with CsA, S3-R significantly decreased the CsA-induced inhibition of MRTF-SRF transcription activity (CsA: −33.1%; S3-R + CsA: −24.5%; +8.6%, *$P < .05$). LIMKi3 alone induced an inhibition of MRTF-SRF transcription activity (Figure 5B, −52.3%, ***$P < .001$) like what was observed with CsA alone (−35.9%, ***$P < .001$). Furthermore, LIMKi3 reinforced the CsA-induced inhibition of SRF transcription activity (−61.5%, ***$P < .001$).

The pharmacological inhibitors of the RhoGTPases pathway, Y27632 (ROCK inhibitor) and EHT1864 (Rac1 inhibitor) elicited the same effects as LIMKi3 at both cytoskeletal (Figure S2A) and transcriptional (Figure S2B) levels.

In conclusion, CsA effects involved the phosphorylation site of CFL as a target for dephosphorylation. Inhibitors of the RhoGTPases pathway triggered CsA-like effects.

3.6 | CsA inhibited Na^+/K^+-ATPase activity in PTCs and Ouabain-induced inhibition of Na^+/K^+-ATPase mimicked actin reorganization and inhibition of MRTF-SRF transcription activity observed upon CsA exposure

Cyclosporine A inhibition of Na^+/K^+-ATPase and actin cytoskeleton reorganization consecutive to Na^+/K^+-ATPase inhibition were reported in other in vivo and in vitro models. To determine whether CsA inhibition of Na^+/K^+-ATPase and Na^+/K^+-ATPase-related actin dynamics occurred in PTC, the Na^+/K^+-ATPase activity of LLC PK-1 cells was measured after 24-hour exposure to CsA and the characterization of LLC PK-1 actin cytoskeleton and MRTF-SRF transcription activity was done after 24 hours exposure to Ouabain, a pharmacological inhibitor of Na^+/K^+-ATPase.

A significant decrease in the Na^+/K^+-ATPase activity (−23.1% of control, **$P < .01$) was observed in LLC PK-1 exposed for 24 hours to CsA (Figure 6A), whereas Tac treatment had no effect.

Lilly Laboratories Porcine Kidney-1 exposed for 24 hours to 100 nmol/L Ouabain featured CsA-like actin reorganization a(Figure 6 B panel c) with a significantly greater loss of F-actin (Figure 6C, CsA: −0.76%; OUA: −1.35%, ***$P < .001$). Moreover, Ouabain cotreatment with CsA potentiated CsA-induced cell stiffening (Figure 6B panel d) and F-actin decrease (Figure 6C, −2.26%, ***$P < .001$). Likewise, Ouabain exposure led to the inhibition of MRTF-SRF transcription activity (Figure 6D, −26.6%). Ouabain cotreatment with CsA reinforced CsA effects (CsA: −47.0%; OUA + CsA: −62.0%, ***$P < .001$).

In conclusion, CsA targeted Na^+/K^+-ATPase and inhibited its activity. Na^+/K^+-ATPase inhibitor Ouabain elicited actin reorganization the same way CsA did. Ouabain-related actin dynamics induced the partial inhibition of MRTF-SRF transcription activity. The association of Ouabain with CsA tended to potentiate CsA effects on tubular proximal morphology and actin dynamics.

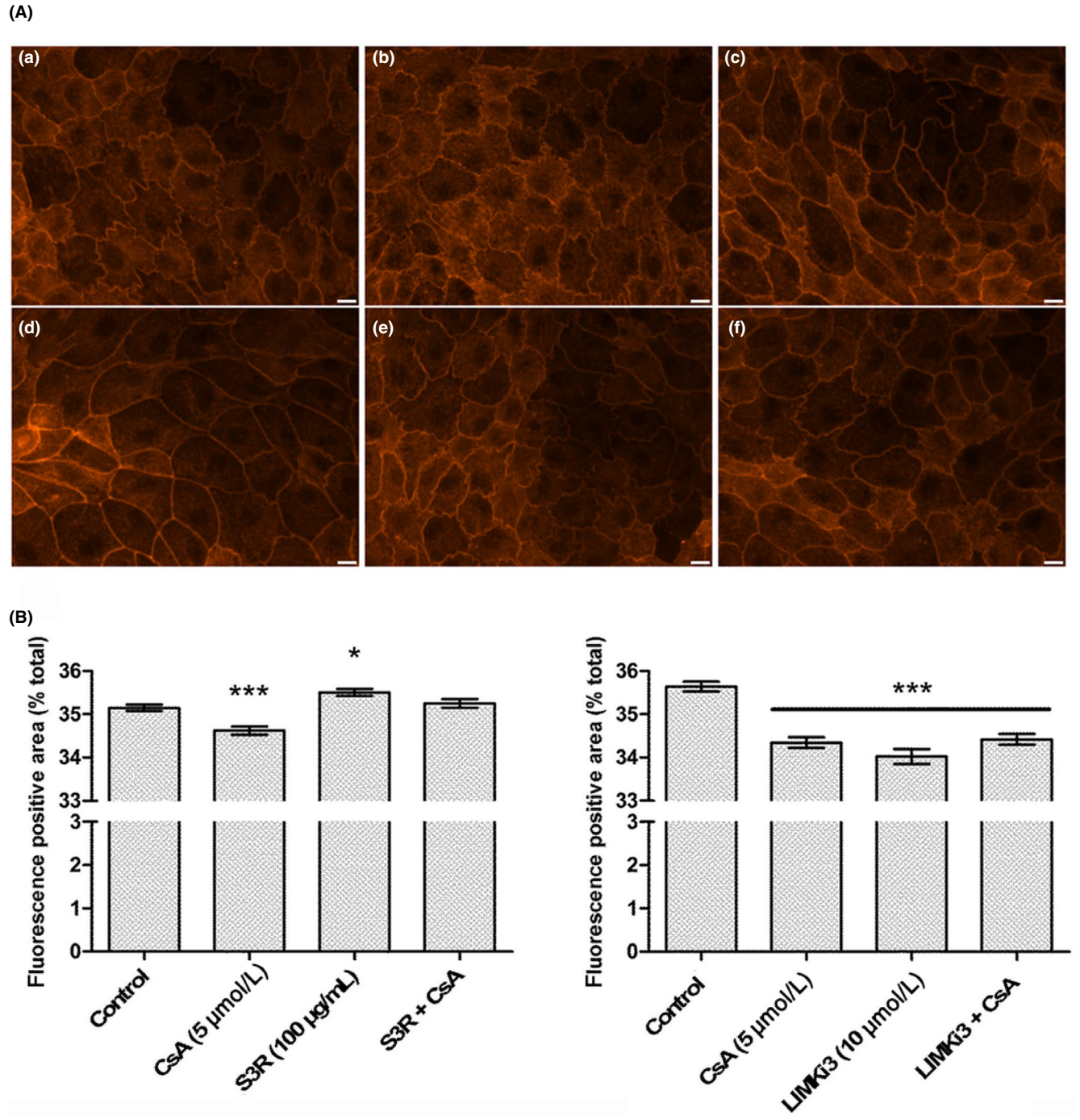

FIGURE 4 Cofilin is involved in cyclosporine A (CsA)-induced actin reorganization through its phosphorylation site. A, Fluorescence images of Lilly Laboratories Porcine Kidney-1 actin cytoskeleton labeled with TRITC-Phalloidin. Scale bar 10 µm. B, Quantification of red fluorescence-positive area. Mean ± SEM. One-way ANOVA plus Tukey's post-test (*$P < .05$, ***$P < .001$) (n = 4). Drug condition: (a) Vehicle (b) 100 µg/mL S3R (c) 10 µmol/L LIMKi3 (d) 5 µmol/L CsA (e) S3R + CsA (f) LIMKi3 + CsA. Exposure time: 24 h (n = 4)

3.7 | CsA molecular docking into Na^+/K^+-ATPase

Cyclosporine A was docked into the closed (E1) conformation of Na^+/K^+-ATPase with and without ATP and into the open (E2) conformation without any ligands (Figure S3). All the obtained binding poses had similar binding affinity, ranging from −7.7 to −6.6 kcal/mol. Assuming the known membrane partitioning of CsA[34,35] only the binding poses close to the membrane boundary were considered.

On the open conformation of Na^+/K^+-ATPase (state E2, Figure S3A), there is a binding site at the C-terminal end of the protein, near the β-subunit, in the vicinity of the C-terminal pathway[36,37] There is another binding site under the

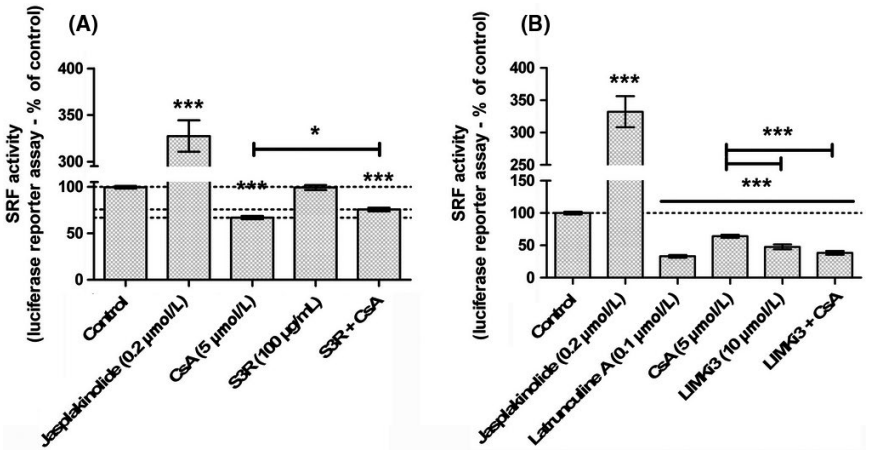

FIGURE 5 Cofilin is involved in cyclosporine A (CsA)-induced inhibition of myocardin-related transcription factors-serum response factor (SRF) transcription activity. SRF transcription activity was measured by luciferase gene reporter assay in Lilly Laboratories Porcine Kidney-1 SRE exposed 24 h to: (A) S3-R 100 µg/mL; S3R + CsA. (n = 6); (B) LIMKi3 10 µmol/L; LIMKi3 + CsA. (n = 7). Mean ± SEM. One-sample *t* test for vs control comparison, One-way ANOVA plus Tukey's post-test for multiple condition comparison (**P* < .01, ****P* < .001)

A-domain. It is noteworthy that this binding site is present in both conformations (Figure S3A and B) and near the binding site of Oligomycin A in the 3WGV crystal structure.[38]

In the closed conformation of Na^+/K^+-ATPase (state E1, Figure S3B and C), the most prominent binding sites are at the lipid-binding sites as previously defined.[39] Most of the binding poses are located at the so-called site C—a position of bound cholesterol and phospholipid, involving aromatic and aliphatic residues such as W32 and Y39 or V838. This site has been previously implicated in the Na^+/K^+-ATPase inhibition.

4 | DISCUSSION

In this work, we demonstrated that CsA-induced remodeling of the actin cytoskeleton of PTC was associated with a modification of the F-actin: G-actin ratio through an original regulation of CFL: Indeed, CsA exposure decreased the total CFL: actin ratio as well as the levels of CFL dimers and tetramers, independently of the phosphorylation by LIM kinases but most likely related to the CsA-induced inhibition of Na^+/K^+-ATPase.

In the kidney, the study of podocytes exposed to CsA revealed that the dynamic of the actin cytoskeleton was sensitive to CsA. Indeed, CsA exerted the stabilization of the actin cytoskeleton of podocyte foot processes, explaining the antiproteinuric effect of CsA which is observed in nephrosis. This mechanism was demonstrated to be calcineurin-dependent with the inhibition of the dephosphorylation and consequent proteolysis of Synaptopodin, a podocyte specific actin-binding protein (ABP) whose activity is essential for podocyte structure-function.[40] Besides, CsA induced the overexpression of CFL, a ubiquitary ABP, and its regulation in a non-phosphorylated state, independently from the effects on Synaptopodin.[41]

In the light of early observations of CsA effects on the actin cytoskeleton of podocytes, the study of the actin dynamic in PTC appeared of utmost interest in the elucidation of pathophysiological mechanisms of TA upon CNI exposure. In PTC, we demonstrated that the actin cytoskeleton could be modified by CsA.[42] Indeed, independently from the inhibition of NFAT, CsA triggered a reversible disorganization of actin scaffolding at the periphery of the cell. Whether a mechanism involving the CsA-related regulation of CFL was responsible for the effects of CsA on PTC remained to be addressed.

Cofilin was initially described as an actin-depolymerizing factor involved in actin treadmilling. CFL modifies the physical-chemical properties of the microfilaments, promotes Pi release and aADP-actin-G dissociation from older segments to replenish the pool of G-actin and to supply enough material for microfilament renewal. Since then, the scope of CFL activity was expanded, in the light of the multiple mechanisms of CFL regulation. Up to date, CFL activity is known to be sensitive to F-actin saturation, phosphorylation-dephosphorylation of its Ser3 residue, PIP2 interaction, intracellular pH, and oxidative stress.[43]

Since direct interaction with F-actin microfilaments is necessary for the actin-related activity CFL, the degree of saturation of the microfilament (or the density of CFL near the microfilament) play a major role in the regulation of CFL. Saturation is correlated with global CFL concentration, CFL: actin ratio and CFL oligomerization. At high saturation and CFL density, F-actin filaments are severed and prone to the nucleation and polymerization of new branches. Conversely, at low saturation and CFL density, F-actin filaments are severed and completely depolymerized into G-actin. Low CFL

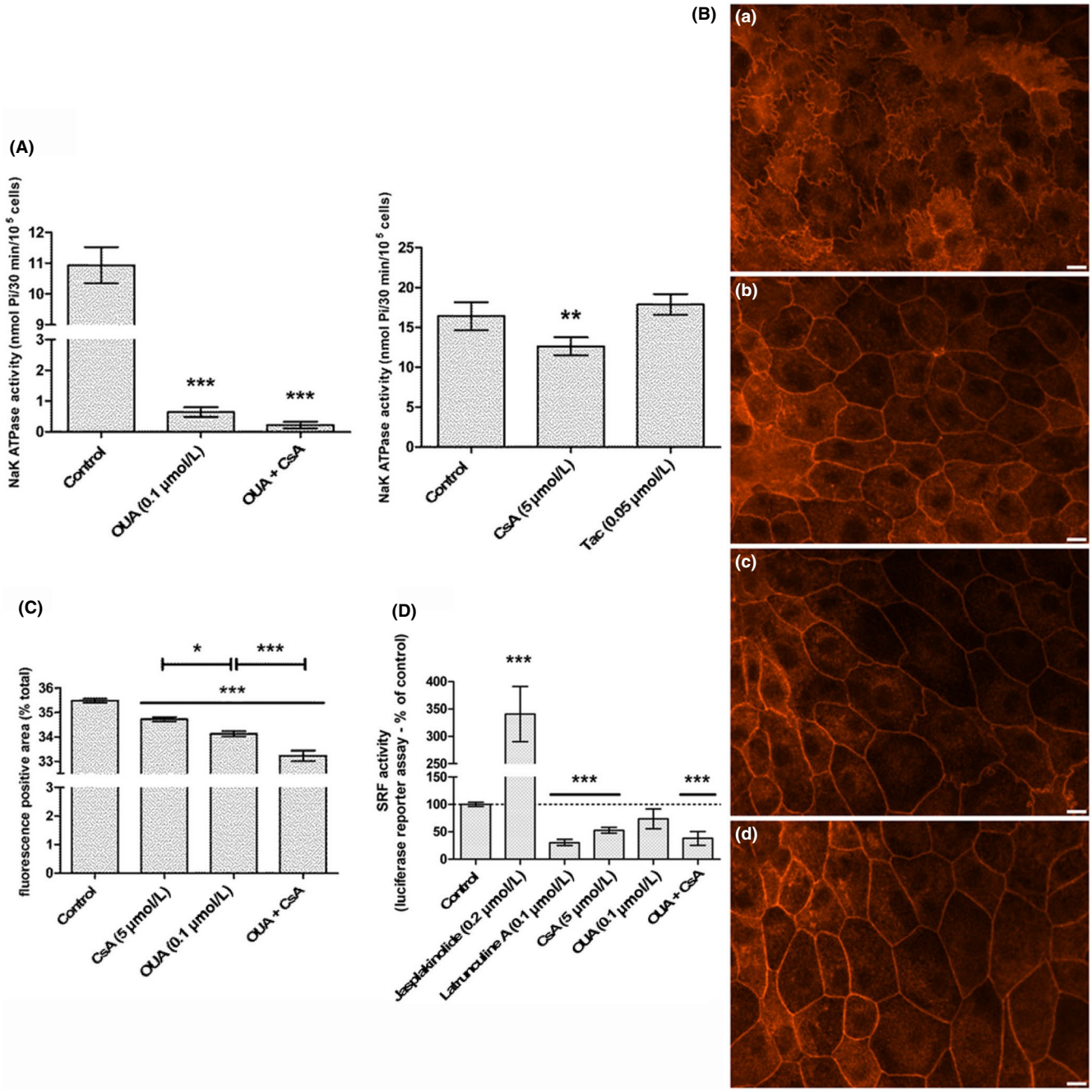

FIGURE 6 Cyclosporine A (CsA) partially inhibits Na^+/K^+-ATPase activity; Na^+/K^+-ATPase inhibitor Ouabain triggers and potentiates CsA-like actin reorganization and inhibition of serum response factor (SRF)-myocardin-related transcription factor transcription transcription activity. A, Na^+/K^+-ATPase activity was measured by colorimetric phosphate assay in Lilly Laboratories Porcine Kidney-1 (LLC PK-1). Mean ± SEM. One-way ANOVA plus Dunn's post-test (**$P < .01$, ***$P < .001$) (n = 3). B, Fluorescence images of LLC PK-1 actin cytoskeleton labeled with TRITC-Phalloidin. Scale bar 10 µm. C, Quantification of red fluorescence-positive area. Mean ± SEM, One-way ANOVA plus Tukey's post-test (*$P < .01$, ***$P < .001$) (n = 4). D, SRF transcription activity was measured by luciferase gene reporter assay in LLC PK-1 SRE. One-sample *t* test for vs control comparison, one-way ANOVA plus Tukey's post-test for multiple condition comparison (***$P < .001$) (n = 4). Drug condition: (a) Vehicle (b) 5 µmol/L CsA (c) 100 nmol/L Ouabain (d) CsA + Ouabain. Exposure time: 24 h

concentrations are related to low saturation, and so, the higher the concentration, the higher the saturation of microfilaments.[44,45] Besides, in vivo and in vitro, CFL may exist as monomers, dimers and tetramers with higher order oligomers related to higher CFL concentration and F-actin saturation.[46,47]

The switches between phosphorylated and dephosphorylated status are another level of regulation between active and inactive CFL. Phosphorylation of the Ser3 residue prevents CFL-actin interaction, whereas dephosphorylation rescues CFL-actin interaction and enables actin-related CFL

activity. Phosphorylation of Ser3 is only catalyzed by LIM kinases, downstream small RhoGTPases and their associated kinases.[48] Dephosphorylation of CFL Ser3 is catalyzed by Slingshot phosphatases,[49] which itself is activated by calcineurin.

The regulation of CFL orientates actin dynamics toward the polymerization of G-actin monomers into F-actin microfilaments, or, conversely, promotes the depolymerization of F-actin into G-actin. In case of a cytoplasmic accumulation of G-actin, G-actin traps myocardin-related transcription factor (MRTF), a co-factor of the serum response factor (SRF) transcription factor. Complexes of MRTF-G-actin are restricted to the cytoplasm. Gene transcription by MRTF-SRF complexes depends on the nuclear import of MRTF hence the cytoplasmic accumulation of G-actin leads to SRF transcription inhibition.[50] In that way, the actin dynamic was described as a potent intracellular fulcrum for cell adaptation to its environment, connecting upstream RhoGTPases to downstream MRTF-SRF pathway.[51-53]

As mentioned above, studies on podocytes reported that CsA had antiproteinuric effects via the stabilization of the actin cytoskeleton structuring the foot processes. This stabilization relied on the overexpression and dephosphorylation of Cofilin. Even though the study did not focus on CFL oligomerization, the CFL: actin ratio was in favor of CFL and the CFL concentration was higher, therefore the activity of CFL was regulated to promote actin polymerization and stabilize microfilaments. What we observed in PTC was a destabilization of the actin cytoskeleton structuring the intercellular convolutions. This indicated a different regulation of CFL activity where CFL would have to (a) exert low saturation of F-actin microfilaments (lower CFL: actin ratio; lower levels of CFL oligomers); (b) be active for actin-related functions, that is, dephosphorylated.

Cyclosporine A had already been reported to elicit the remodeling of the actin cytoskeleton of PTC.[54] In this study, CsA (4.2 μmol/L, 24 hours) activated RhoA and the phosphorylation cascade, which led to CFL phosphorylation by LIMK. CFL inhibition results in the formation of stress fibers and the tightening of tight junctions. Our findings are just the opposite of these previous results and are incompatible with the previously described mechanism. Indeed, pharmacological inhibition of the RhoGTPases pathway elicited CsA-like effects, that is, the loss of proximal tubular morphology and the inhibition of MRTF-SRF activity. These discrepancies might result from differences in cell culture conditions as, in the study by Martin-Martin et al, control LLC PK-1 seemed non-confluent, less differentiated, with non-convoluted membranes and a significant amount of stress fibers. Although the cell culture protocol appeared to be similar, the serum deprivation prior to drug exposure differed as it is not supplemented with hormones allowing advanced epithelial differentiation of LLC PK-1 cells at the morphological and cytoskeletal levels. Our present in vitro model seemed closer to the in vivo aspect of PTC than the in vitro one Martin-Martin et al developed.

Outside actin-related functions, CFL is known to interact with Na^+/K^+-ATPase to provide energetic fuel to the pump motion. CFL binds triose phosphate isomerase and interacts with the alpha subunit of Na^+/K^+-ATPase to locally provide ATP. When Na^+/K^+-ATPase is inhibited (by potassium depletion or the action of a pharmacological inhibitor), a feedback mechanism disrupts energetic supply by CFL dephosphorylation.[55-57]

Cyclosporine A effects on PTCs were reminiscent of OUA effects on HeLa cells.[55] OUA exerted a similar reorganization of the actin cytoskeleton by dephosphorylating CFL via a mechanism where the inhibition of Na^+/K^+-ATPase activates the Ras/Raf/MEK cascade, in a Src-EGFR-dependent way, leading to the inhibition of LIMK downstream the small RhoGTPases pathway. OUA effects were reproduced by Y27632 just like CsA effects were mimicked by the RhoGTPases inhibitors.

Earlier findings about the mechanism of Na^+/K^+-ATPase energetic supply by pCFL-TPI complexes[57] reported that the overexpression of constitutively active CFL (Ser3 was replaced by Ala) was sufficient to cut endogenous CFL out of phosphorylation/dephosphorylation-based regulation which made TPI localization insensitive to the activation/inhibition of the RhoGTPases pathway. Likewise, in our study, the addition of S3-R was enough to partially exclude endogenous CFL from CsA-induced regulation.

Dephosphorylation of CFL by Slingshot phosphatases seemed unlikely since Slingshot phosphatases are activated by calcineurin. CsA effects on CFL were unlikely to be related to calcineurin since Tac and VIVIT did not elicit CsA-like effects on the actin cytoskeleton or the MRTF-SRF transcription activity.

Numerous studies have already reported the inhibition of Na^+/K^+-ATPase by CsA, in vitro and in vivo. However, the observations were limited to the consequences in ion transport.[58-65] Although this work is not the first one to study the relationship between the Na^+/K^+-ATPase pump and the actin cytoskeleton, the partial inhibition (about 25%) of proximal tubular Na^+/K^+-ATPase by CsA has been the first observation of a direct correlation between variations in the pump activity and cytoskeletal remodeling so far. Besides, the potentiation of the CsA-induced depolymerization of F-actin by OUA is in favor of a Na^+/K^+-ATPase -related mechanism.

How CsA inhibits Na^+/K^+-ATPase has yet to be elucidated. CsA is known to induce overexpression of endothelin, which is a well-known inhibitor of Na^+/K^+-ATPase activity.[66,67] Furthermore, CsA can downregulate Na^+/K^+-ATPase activity through the inhibition of cyclophilin B. The PPIase was described as a crucial partner for the structure and activity of Na^+/K^+-ATPase catalytic subunit.[68] Besides, the

proteome monitoring of HEK cells by SILAC-LC-MS/MS reported the decrease in CypB protein abundance upon CsA exposure.[69] These findings, together with the observations of CsA-like effects upon CAI exposure, support the implication of Cyps in the inhibition of Na^+/K^+-ATPase by CsA. To what extent the Cyps are implicated has yet to be elucidated. However, our work suggests another mechanism leading to Na^+/K^+-ATPase inhibition.

Indeed, our molecular modeling of CsA docking into Na^+/K^+-ATPase was performed to visualize the potential interactions. CsA is mostly made of hydrophobic amino acids favoring its membrane partitioning.[34] Therefore, the preferential binding site to Na^+/K^+-ATPase is likely to be in the transmembrane site C, known to bind hydrophobic compounds such as lipids and cholesterol. Such binding is mostly expected to hinder proper motions of the transmembrane helices by impairing specific protein-lipid interactions. This may explain the experimentally observed inhibition of Na^+/K^+-ATPase by CsA given that the Na^+/K^+-ATPase (a) undergoes large-scale conformational changes during its reaction cycle; and (b) its activity is strongly dependent of the membrane environment.[70] Interestingly, in the open structure, there are no binding sites in the transmembrane region, but there are two at the membrane interface that could (a) impair domain motions; and (b) prevent the proper closing of N- and A- domains during the reaction cycle. It is noteworthy that there is also a binding site under the A-domain, similar to the one in the closed conformation. Such preliminary results are in favor of direct interactions between CsA and Na^+/K^+-ATPase leading to impairment of large-scale conformational motions. It is important to note that the confirmation of the aforementioned molecular mechanism would require an important computational effort by biased molecular dynamics simulations, which if off-topic of this study.

Altogether, these results let us propose a model (Figure 7) where: (a) the inhibition of Na^+/K^+-ATPase by CsA leads to the dephosphorylation of CFL, independently from the classical regulation pathways; (b) CsA decreases the CFL:

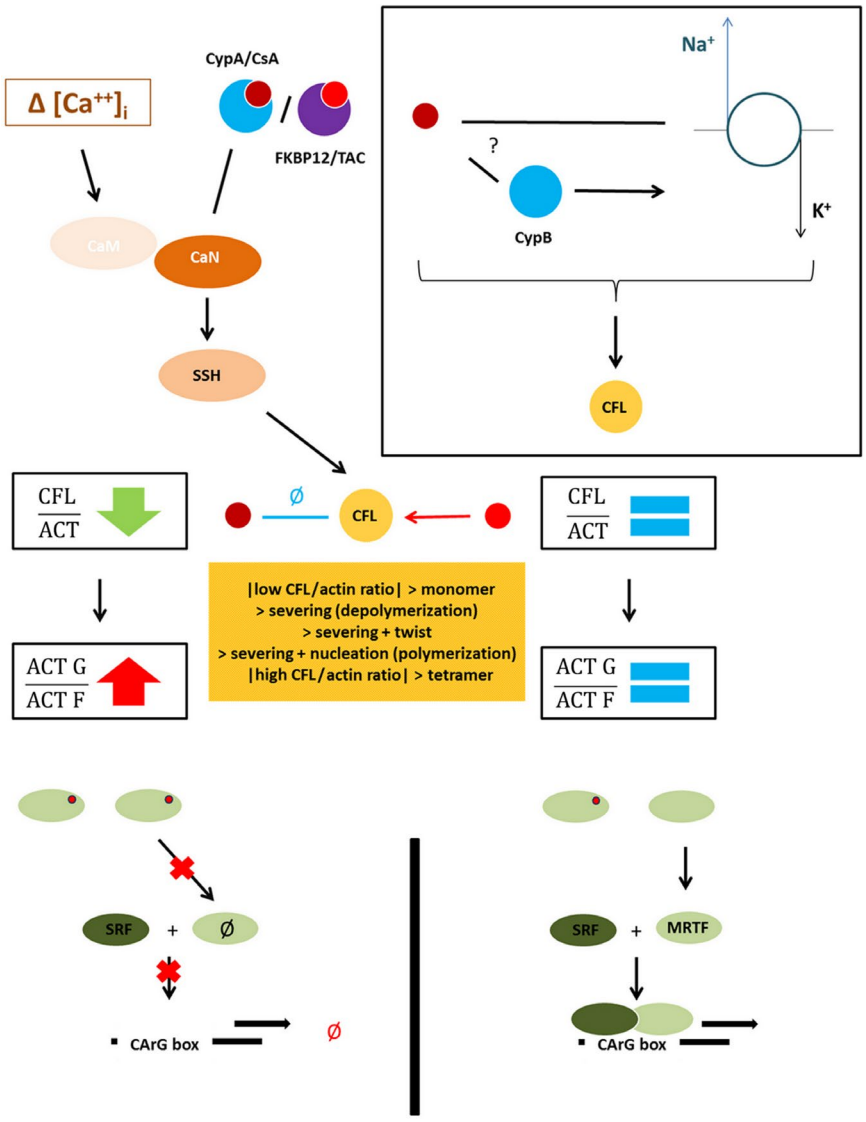

FIGURE 7 Proposed model of cyclosporine A (CsA)-induced myocardin-related transcription factors-serum response factor (MRTF-SRF) inhibition through Na^+/K^+-ATPase inhibition and remodeling of the actin cytoskeleton

actin ratio and the protein abundance of F-actin-stabilizing and polymerization-promoting CFL oligomers; (c) active, minority, monomeric CFL depolymerizes low-saturated F-actin microfilaments and replenish G-actin pools; (d) the accumulation of G-actin leads to the cytoplasmic trapping of the SRF co-factor MRTF; (e) the low nuclear abundance of MRTF results in the low abundance of transcription-ready MRTF-SRF complexes and the decrease in MRTF-SRF transcription activity; overall; (f) CsA inhibits gene transcription by the MRTF-SRF complex via drug-specific, G-actin-prone actin-dynamics.

The CsA-induced inhibition of MRTF-SRF gene transcription might have feedback consequences on actin dynamics since ACTB, Cfl1, and other ABP-coding genes are identified genes of the CArGome (the ensemble of MRTF-SRF genes whose promoters contain CArG boxes) and the activity of the MRTF-SRF complex was shown to be required for the homeostasis of actin levels and the organization of the actin cytoskeleton.[71]

As a matter of facts, cellular consequences of MRTF-SRF inhibition might be large-scale perturbations since MRTF-SRF regulates the transcription of genes coding for transport and adhesion proteins, enzymes of the lipid and glucose metabolisms, transcription factors, growth factors, growth factor receptors, etc.

For instance, past studies clearly elucidated the role of MRTF-SRF inhibition in multifactorial biological processes like proapoptotic mechanisms[72,73] and EMT,[74,75] which have been widely described as CsA-related pathophysiological mechanisms.

Hence why the proposed model of an inhibition of MRTF-SRF transcription activity downstream an original regulation of actin dynamics upon CsA exposure might be of utmost interest to explain known in vitro effects of CsA and provide a unified mechanism of CsA toxicity in PTC.

ACKNOWLEDGEMENTS

This research was partially supported by the grant No. LO1204 (Sustainable development of research in the Centre of the Region Haná) from the National Program of Sustainability I, MEYS.

CONFLICT OF INTEREST

Authors declare that they have no conflict of interest.

AUTHOR CONTRIBUTIONS

BB and ME planned and designed the study. BB designed, performed and analyzed cell biology and molecular biology experiments with HA, QF (Cofilin oligomer cross-linking and Western blotting/ Na^+/K^+-ATPase activity measurement) and FLS (iTRAQ shotgun proteomics). PC and FDM designed, performed and analyzed molecular modeling experiments. BB wrote the manuscript. All authors reviewed and edited the manuscript.

REFERENCES

1. Calne R, Thiru S, Mcmaster P, et al. Cyclosporin A in patients receiving renal allografts from cadaver donors. *Lancet*. 1978;312:1323-1327.
2. Calne RY, Rolles K, Thiru S, et al. Cyclosporin a initially as the only immunosuppressant in 34 recipients of cadaveric organs: 32 kidneys, 2 pancreases, and 2 livers. *Lancet*. 1979;314:1033-1036.
3. Starzl T, Fung J, Venkataramman R, Todo S, Demetris A, Jain A. Fk 506 for liver, kidney, and pancreas transplantation. *Lancet*. 1989;334:1000-1004.
4. Hart A, Smith JM, Skeans MA, et al. Kidney. *Am J Transplant*. 2016;16:11-46.
5. Hart A, Smith JM, Skeans MA, et al. OPTN/SRTR 2015 annual data report: kidney. *Am J Transplant*. 2017;17:21-116.
6. Myers BD, Ross J, Newton L, Luetscher J, Perlroth M. Cyclosporine-associated chronic nephropathy. *N Engl J Med*. 1984;311:699-705.
7. Gaston RS. Chronic calcineurin inhibitor nephrotoxicity: reflections on an evolving paradigm. *Clin J Am Soc Nephrol*. 2009;4:2029-2034.
8. Naesens M, Kuypers D, Sarwal M. Calcineurin inhibitor nephrotoxicity. *Clin J Am Soc Nephrol*. 2009;4:481-508. http://cjasn.asnjournals.org/cgi/doi/10.2215/CJN.04800908. Accessed March 31, 2017.
9. Healy E, Dempsey M, Lally C, Ryan MP. Apoptosis and necrosis: mechanisms of cell death induced by cyclosporine A in a renal proximal tubular cell line. *Kidney Int*. 1998;54:1955-1966.
10. Ito H, Kasagi N, Shomori K, Osaki M, Adachi H. Apoptosis in the human allografted kidney. Analysis by terminal deoxynucleotidyl transferase-mediated DUTP-botin nick end labeling. *Transplantation*. 1995;60:794-798.
11. Jennings P, Koppelstaetter C, Aydin S, et al. Cyclosporine A induces senescence in renal tubular epithelial cells. *Am J Physiol Renal Physiol*. 2007;293:F831-F838.
12. Justo P. Intracellular mechanisms of cyclosporin A-induced tubular cell apoptosis. *J Am Soc Nephrol*. 2003;14:3072-3080.
13. Lally C, Healy E, Ryan MP. Cyclosporine A-induced cell cycle arrest and cell death in renal epithelial cells. *Kidney Int*. 1999;56:1254-1257.
14. Ortiz A, Lorz C, Catalán M, Ortiz A, Coca S, Egido J. Cyclosporine A induces apoptosis in murine tubular epithelial cells: role of caspases. *Kidney Int Suppl*. 1998;68:S25-29.
15. Hama T, Nakanishi K, Mukaiyama H, et al. Endoplasmic reticulum stress with low-dose cyclosporine in frequently relapsing nephrotic syndrome. *Pediatr Nephrol*. 2013;28:903-909.
16. Han SW, Li C, Ahn KO, et al. Prolonged endoplasmic reticulum stress induces apoptotic cell death in an experimental model of chronic cyclosporine nephropathy. *Am J Nephrol*. 2008;28:707-714.
17. Pallet N, Bouvier N, Bendjallabah A, et al. Cyclosporine-induced endoplasmic reticulum stress triggers tubular phenotypic changes and death. *Am J Transplant*. 2008a;8:2283-2296.
18. Pallet N, Bouvier N, Legendre C, et al. Autophagy protects renal tubular cells against cyclosporine toxicity. *Autophagy*. 2008b;4:783-791.

19. Pallet N, Rabant M, Xu-Dubois Y-C, et al. Response of human renal tubular cells to cyclosporine and sirolimus: a toxicogenomic study. *Toxicol Appl Pharmacol*. 2008c;229:184-196.
20. Djamali A. Oxidative stress as a common pathway to chronic tubulointerstitial injury in kidney allografts. *Am J Physiol Renal Physiol*. 2007;293:F445-F455.
21. Vetter M, Chen Z-J, Chang G-D, Che D, Liu S, Chang C-H. Cyclosporin A disrupts bradykinin signaling through superoxide. *Hypertension*. 2003;41:1136-1142.
22. Heering P, Grabensee B. Influence of ciclosporin A on renal tubular function after kidney transplantation. *Nephron*. 1991;59:66-70.
23. Hazzan M, Hertig A, Buob D, et al. Epithelial-to-mesenchymal transition predicts cyclosporine nephrotoxicity in renal transplant recipients. *J Am Soc Nephrol*. 2011;22:1375-1381.
24. McMorrow T, Gaffney MM, Slattery C, Campbell E, Ryan MP. Cyclosporine A induced epithelial-mesenchymal transition in human renal proximal tubular epithelial cells. *Nephrol Dial Transplant*. 2005;20:2215-2225.
25. Slattery C, Campbell E, McMorrow T, Ryan MP. Cyclosporine A-induced renal fibrosis. *Am J Pathol*. 2005;167:395-407.
26. Muth T, Keller D, Puetz SM, Martens L, Sickmann A, Boehm AM. jTraqX: a free, platform independent tool for isobaric tag quantitation at the protein level. *Proteomics*. 2010;10:1223-1225.
27. Deutsch EW, Csordas A, Sun Z, et al. The ProteomeXchange consortium in 2017: supporting the cultural change in proteomics public data deposition. *Nucleic Acids Res*. 2017;45:D1100-D1106.
28. Vizcaíno JA, Csordas A, del-Toro N, et al. 2016 update of the PRIDE database and its related tools. *Nucleic Acids Res*. 2016;44:D447-D456.
29. Shinoda T, Ogawa H, Cornelius F, Toyoshima C. Crystal structure of the sodium–potassium pump at 2.4 Å resolution. *Nature*. 2009;459:446-450.
30. Nyblom M, Poulsen H, Gourdon P, et al. Crystal structure of Na^+, K^+ -ATPase in the Na^+ -bound state. *Science*. 2013;342:123-127.
31. Morris GM, Huey R, Lindstrom W, et al. AutoDock4 and AutoDockTools4: Automated docking with selective receptor flexibility. *J Comput Chem*. 2009;30:2785-2791.
32. Trott O, Olson AJ. AutoDock Vina: improving the speed and accuracy of docking with a new scoring function, efficient optimization, and multithreading. *J Comput Chem*. 2010;31:455–461.
33. Salentin S, Schreiber S, Haupt VJ, Adasme MF, Schroeder M. PLIP: fully automated protein–ligand interaction profiler. *Nucleic Acids Res*. 2015;43:W443-W447.
34. Haynes M, Fuller L, Haynes DH, Miller J. Cyclosporin partitions into phospholipid vesicles and disrupts membrane architecture. *Immunol Lett*. 1985;11:343-349.
35. Wang CK, Swedberg JE, Harvey PJ, Kaas Q, Craik DJ. Conformational flexibility is a determinant of permeability for cyclosporin. *J Phys Chem B*. 2018;122:2261-2276.
36. Čechová P, Berka K, Kubala M. Ion pathways in the Na^+/K^+ -ATPase. *J Chem Inf Model*. 2016;56:2434-2444.
37. Poulsen H, Khandelia H, Morth JP, et al. Neurological disease mutations compromise a C-terminal ion pathway in the Na+/K+-ATPase. *Nature*. 2010;467:99-102.
38. Kanai R, Ogawa H, Vilsen B, Cornelius F, Toyoshima C. Crystal structure of a Na+-bound Na+, K+-ATPase preceding the E1P state. *Nature*. 2013;502:201-206.
39. Cornelius F, Habeck M, Kanai R, Toyoshima C, Karlish S. General and specific lipid–protein interactions in Na, K-ATPase. *Biochim Biophys Acta Biomembr*. 2015;1848:1729-1743.
40. Faul C, Donnelly M, Merscher-Gomez S, et al. The actin cytoskeleton of kidney podocytes is a direct target of the antiproteinuric effect of cyclosporine A. *Nat Med*. 2008;14:931-938.
41. Li X, Zhang X, Li X, Wang X, Wang S, Ding J. Cyclosporine A protects podocytes via stabilization of cofilin-1 expression in the unphosphorylated state. *Exp Biol Med*. 2014;239:922-936.
42. Descazeaud V, Mestre E, Marquet P, Essig M. Calcineurin regulation of cytoskeleton organization: a new paradigm to analyse the effects of calcineurin inhibitors on the kidney. *J Cell Mol Med*. 2012;16:218-227.
43. Vantroys M, Huyck L, Leyman S, Dhaese S, Vandekerkhove J, Ampe C. Ins and outs of ADF/cofilin activity and regulation. *Eur J Cell Biol*. 2008;87:649-667.
44. Andrianantoandro E, Pollard TD. Mechanism of actin filament turnover by severing and nucleation at different concentrations of ADF/cofilin. *Mol Cell*. 2006;24:13-23.
45. Yeoh S, Pope B, Mannherz HG, Weeds A. Determining the differences in actin binding by human ADF and cofilin1. *J Mol Biol*. 2002;315:911-925.
46. Goyal P, Pandey D, Brünnert D, Hammer E, Zygmunt M, Siess W. Cofilin oligomer formation occurs in vivo and is regulated by cofilin phosphorylation. *PLoS ONE*. 2013;8:e71769.
47. Pfannstiel J, Cyrklaff M, Habermann A, et al. Human cofilin forms oligomers exhibiting actin bundling activity. *J Biol Chem*. 2001;276:49476-49484.
48. Geneste O, Copeland JW, Treisman R. LIM kinase and diaphanous cooperate to regulate serum response factor and actin dynamics. *J Cell Biol*. 2002;157:831-838.
49. Huang TY, DerMardirossian C, Bokoch GM. Cofilin phosphatases and regulation of actin dynamics. *Curr Opin Cell Biol*. 2006;18:26-31.
50. Miralles F, Posern G, Zaromytidou A-I, Treisman R. Actin Dynamics control SRF activity by regulation of its coactivator MAL. *Cell*. 2003;113:329-342.
51. Hill CS, Wynne J, Treisman R. The Rho family GTPases RhoA, Racl, and CDC42Hsregulate transcriptional activation by SRF. *Cell*. 1995;81:1159-1170.
52. Maekawa M. Signaling from Rho to the actin cytoskeleton through protein kinases ROCK and LIM-kinase. *Science*. 1999;285:895-898.
53. Sotiropoulos A, Gineitis D, Copeland J, Treisman R. Signal-regulated activation of serum response factor is mediated by changes in actin dynamics. *Cell*. 1999;98:159-169.
54. Martin-Martin N, Dan Q, Amoozadeh Y, et al. RhoA and Rho kinase mediate cyclosporine A and sirolimus-induced barrier tightening in renal proximal tubular cells. *Int J Biochem Cell Biol*. 2012;44:178-188.
55. Jung J, Kim M, Choi S, et al. Molecular mechanism of cofilin dephosphorylation by ouabain. *Cell Signal*. 2006a;18:2033-2040.
56. Jung J, Park H, Kim M, Kim M-J, Choi EC, Lee K. Extracellular potassium deprivation reversibly dephosphorylates cofilin. *Biochem Biophys Res Commun*. 2006;345:1393-1397.
57. Jung J, Yoon T, Choi EC, Lee K. Interaction of cofilin with triose-phosphate isomerase contributes glycolytic fuel for Na, K-ATPase via Rho-mediated signaling pathway. *J Biol Chem*. 2002;277:48931-48937.

58. Deppe CE, Heering PJ, Tinel H, Kinne-Saffran E, Grabensee B, Kinne RK. Effect of cyclosporine A on Na+/K(+)-ATPase, Na+/K+/2Cl- cotransporter, and H+/K(+)-ATPase in MDCK cells and two subtypes, C7 and C11. *Exp Nephrol*. 1997;5:471-480.
59. Ferrer-Martínez A, Felipe A, Barceló P, Casado FJ, Ballarín J, Pastor-Anglada M. Effects of cyclosporine A on Na, K-ATPase expression in the renal epithelial cell line NBL-1. *Kidney Int*. 1996;50:1483-1489.
60. Ihara H, Hosokawa S, Ogino T, Arima M, Ikoma F. Activation of K+ channel and inhibition of Na(+)-K+ ATPase of human erythrocytes by cyclosporine: possible role in hyperpotassemia in kidney transplant recipients. *Transplant Proc*. 1990;22:1736-1739.
61. Lea JP, Sands JM, McMahon SJ, Tumlin JA. Evidence that the inhibition of Na+/K+-ATPase activity by FK506 involves calcineurin. *Kidney Int*. 1994;46:647-652.
62. Marakhova I, Ivanova A, Toropova F, Vereninov A, Vinogradova T. Functional expression of the Na/K pump is controlled via a cyclosporin A-sensitive signalling pathway in activated human lymphocytes. *FEBS Lett*. 1999;456:285-289.
63. Marakhova II, Vereninov AA, Vinogradova TA, Toropova FV. Cyclosporin A inhibits long-term activation of Na+, K+ pump in phytohemagglutinin-stimulated human lymphocytes. *Membr Cell Biol*. 1998;12:363-374.
64. Tumlin JA, Sands JM. Nephron segment-specific inhibition of Na+/K+-ATPase activity by cyclosporin A. *Kidney Int*. 1993;43:246-251.
65. Younes-Ibrahim M, Barnese M, Burth P, Castro-Faria MV. Inhibition of purified human kidney Na^+, K^+ -ATPase by cyclosporine A. *Ann N Y Acad Sci*. 2003;986:633-635.
66. Nakahama H. Stimulatory effect of cyclosporine A on endothelin secretion by a cultured renal epithelial cell line, LLC-PK1 cells. *Eur J Pharmacol*. 1990;180:191-192.
67. Zeidel ML, Brady HR, Kone BC, Gullans SR, Brenner BM. Endothelin, a peptide inhibitor of Na(+)-K(+)-ATPase in intact renaltubular epithelial cells. *Am J Physiol Cell Physiol*. 1989;257:C1101-C1107.
68. Suñé G, Sarró E, Puigmulé M, et al. Cyclophilin B interacts with sodium-potassium ATPase and is required for pump activity in proximal tubule cells of the kidney. *PLoS ONE*. 2010;5:e13930.
69. Lamoureux F, Mestre E, Essig M, Sauvage FL, Marquet P, Gastinel LN. Quantitative proteomic analysis of cyclosporine-induced toxicity in a human kidney cell line and comparison with tacrolimus. *J Proteomics*. 2011;75:677-694.
70. Bhatia T, Cornelius F, Brewer J, et al. Spatial distribution and activity of Na+/K+ -ATPase in lipid bilayer membranes with phase boundaries. *Biochim Biophys Acta Biomembr*. 2016;1858:1390-1399.
71. Sun Q. Defining the mammalian CArGome. *Genome Res*. 2005;16:197-207.
72. Cao X-L, Hu X-M, Hu J-Q, Zheng W-X. Myocardin-related transcription factor-A promoting neuronal survival against apoptosis induced by hypoxia/ischemia. *Brain Res*. 2011;1385:263-274.
73. Sisson TH, Ajayi IO, Subbotina N, et al. Inhibition of myocardin-related transcription factor/serum response factor signaling decreases lung fibrosis and promotes mesenchymal cell apoptosis. *Am J Pathol*. 2015;185:969-986.
74. Gasparics Á, Sebe A. MRTFs- master regulators of EMT: MRTFs-master regulators of EMT. *Dev Dyn*. 2018;247:396-404.
75. Korol A, Taiyab A, West-Mays JA. RhoA/ROCK signaling regulates TGFβ-induced epithelial-mesenchymal transition of lens epithelial cells through MRTF-A. *Mol Med*; 2016:22:713-723.

SUPPORTING INFORMATION

Additional supporting information may be found online in the Supporting Information section at the end of the article.

How to cite this article: Burat B, Faucher Q, Čechová P, et al. Cyclosporine A inhibits MRTF-SRF signaling through Na^+/K^+ ATPase inhibition and actin remodeling. *FASEB BioAdvances*. 2019;1:561–578. https://doi.org/10.1096/fba.2019-00027